Supramolecular Materials 2 (2023) 100042

Contents lists available at ScienceDirect

Supramolecular Materials

journal homepage: www.keaipublishing.com/en/journals/supramolecular-materials/

# Well-Tunable, 3D-printable, and Fast Autonomous Self-Healing Elastomers

Bingrui Li [a], Sirui Ge [b], Xiao Zhao [c], Qiyi Chen [d], Jia Tian [g], Diana Hun [e], Alexei P. Sokolov [c,f], Tomonori Saito [a,c,*], Peng-Fei Cao [g,**]

[a] The Bredesen Center for Interdisciplinary Research and Graduate Education, University of Tennessee, Knoxville, Tennessee 37996, United States
[b] Department of Material Science and Engineering, University of Tennessee, Knoxville, Tennessee 37996, United States
[c] Chemical Sciences Division, Oak Ridge National Laboratory, Oak Ridge, Tennessee 37830, United States
[d] Center for Nanophase Materials and Sciences, Oak Ridge National Laboratory, Oak Ridge, Tennessee 37830, United States
[e] Buildings and Transportation Science Division, Oak Ridge National Laboratory, Oak Ridge, Tennessee 37830, United States
[f] Department of Chemistry, University of Tennessee, Knoxville, Tennessee 37996, United States
[g] State Key Laboratory of Organic-Inorganic Composites, Beijing University of Chemical Technology, Beijing 100029, PR China

ARTICLE INFO

*Keywords:*
Self-healing, Elastomer
Tunable mechanical properties
Hydrogen bonding
3d printing

ABSTRACT

Self-healing elastomers provide extended longevity of functional materials, due to their unique adaptability and durability. However, a major scientific challenge remains in developing materials with a rapid healing process combined with decent mechanical properties, that can be prepared by a relatively simple synthesis approach. Herein, we report a versatile design approach on self-healing elastomers by incorporating two different hydrogen bonding containing monomers, i.e., 2-[[(butylamino)carbonyl]oxy]ethyl acrylate (BCOE) and 2-ureido-4[1*H*] pyrimidinone (UPy) functionalized ethyl methacrylate. Poly(BCOE-*r*-UPy)s are synthesized by reversible addition−fragmentation chain-transfer (RAFT) polymerization, and controlling the ratio of two monomers enables well-tunable mechanical properties with tensile strength ranging from 0.04 to 6.3 MPa and tensile strain up to 3,000 %. The characteristic dissociation energy is calculated from a temperature dependence of terminal relaxation followed by subtracting the segmental relaxation. The rapid autonomous self-healing is achieved when the molar composition of Poly(BCOE-*r*-UPy) is tailored to BCOE/UPy = 99/1. The self-healing process is monitored *in situ* by a helium-ion microscope, and its macroscopic study using tensile tests indicates that Poly (BCOE-*r*-UPy1) with 1 % molar ratio of UPy recovers 70 % of its original toughness at ambient temperature within 10 mins. 3D printing of Poly(BCOE-*r*-UPy) affords a self-healable 3D structure, demonstrating the adaptability of Poly(BCOE-*r*-UPy) for on-demand fabrication. The simplicity of synthesis, well-tunable mechanical properties, unique self-healability, and 3D printing capability of Poly(BCOE-*r*-UPy)s indicate their potential for a range of applications.

## 1. Introduction

The self-healing feature of human skin achieves restoration of functionalities within a few weeks, providing repeatable protection against injuries. Adopting the concept from nature, the integrated self-healability in synthetic polymers endows improved adaptability and longevity in various applications including coatings [1–3], electrodes [4–6], sensors [7–9], gas-separation membranes [10,11], and healable sealants [12,13], etc. There are two general approaches to achieve self-healability for polymeric materials. One approach typically introduces two reactive chemicals under physical confinement to the polymer matrix that could physically mix and react upon damage [14], and the product of those rapid chemical reactions could seal the void [15]. Although such an approach is more accessible due to its long development history, its key drawback is its one-time healing feature along with some concerns about the complexity of packaging, which requires optimum isolation between reactants. Another approach, where polymer materials rely on dynamic reversible bonds and efficient chain dynamics internally, provides a distinctive advantage of repeated healing. Such design of self-healable polymers consists of a broad range of variables [16–21], including types of reversible covalent bonds such as Diels–Alder reaction [22,23], reversible disulfide bond [24,25], and

* Corresponding authors at: Tomonori Saito, PO Box 2008, MS6210, Oak Ridge, TN 37831-6210, USA.
** Corresponding author at: Beijing University of Chemical Technology, Beijing 10029, PR China.
*E-mail addresses:* saitot@ornl.gov (T. Saito), caopf@buct.edu.cn (P.-F. Cao).

https://doi.org/10.1016/j.supmat.2023.100042
Received 18 August 2023; Received in revised form 28 September 2023; Accepted 28 September 2023
Available online 11 October 2023
2667-2405/© 2023 The Author(s). Published by Elsevier B.V. on behalf of KeAi Communications Co., Ltd. This is an open access article under the CC BY-NC-ND license (http://creativecommons.org/licenses/by-nc-nd/4.0/).

boronic esters [26] along with noncovalent bonds, such as metal-ligand coordination [27], ionic bond [28–30], and hydrogen bonding (H-bonding) [10,25,31].

Stretchable materials provide good adaptability against mechanical deformation. Such high-performance stretchable materials enable the development of attachable devices, flexible electronics, personal protection devices, and healable materials for building envelope [32]. Integration of self-healing character into a stretchable material is especially beneficial since it could dramatically increase their ductility and reliability [10,13,33]. The advancement of stretchable self-healing materials shows great potential under multiple scenarios such as conductive materials [34,35], sensing devices [36,37], coatings [38], supercapacitors [39], sealants [13], and electronic skins [40], since self-healing materials could facilitate the recovery of functionalities by rebuilding physical contact between the damaged sections. Yet many reported materials still suffer from several drawbacks. Firstly, the low mechanical strength of most self-healing elastomers limits their utilization as a structural material [41,42]. This is especially true for those autonomous self-healing elastomers that heal at ambient temperature, and their ultimate mechanical stress and modulus almost always reside in the range of kPa. On the other hand, mechanically robust self-healing elastomers typically require elevated temperatures or prolonged time at room temperature (RT) to achieve complete property recovery [1,43,44]. Such trade-off between the rate of self-healing and mechanical strength deteriorates the product's healing performance [16], since temperature beyond ambient temperature may not be easily obtained in many scenarios, such as building roofs and sealants, aerospace, and deep-sea devices. Additionally, self-healing time is equally critical during the evaluation of self-healing polymers. Although many results demonstrated almost 100 % property recovery in hours, polymers with adequate property recovery at less than 30 min of healing time are still rarely reported. Thus, developing a rapid, autonomous self-healable elastomer with improved mechanical performance is highly desirable for many applications [45,46].

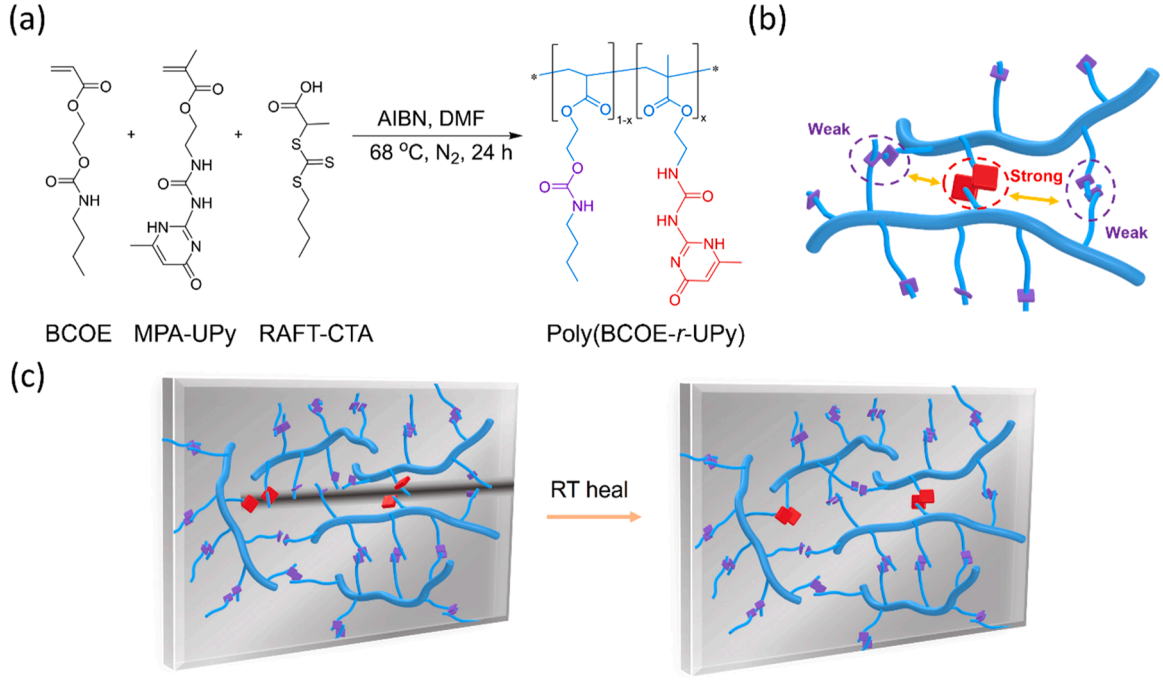
Herein, we report a series of autonomous self-healable copolymer elastomers (ASCEs) with tunable mechanical properties *via* a facile copolymerization with monomers of different H-bond strengths, i.e., 2-[[(butylamino)carbonyl]oxy]ethyl acrylate (BCOE) and 2-(3-(6-methyl-4-oxo-1,4-dihydropyrimidin-2-yl)ureido)ethyl methacrylate (UPy). With abundant H-bonding units and fast segmental dynamics, the copolymer Poly(BCOE-*r*-UPy) exhibits rapid, autonomous self-healability at ambient temperature, i.e., recovery of 70 % toughness in 10 mins. The in-situ self-healing process of Poly(BCOE-*r*-UPy) is successfully visualized by a helium ion microscope at the micrometer level. The self-healing kinetic and molecular-level healing mechanisms are revealed by tensile test and broadband dielectric spectroscopy, respectively. In addition, the additive manufacturing of Poly(BCOE-*r*-UPy) to 3D objects is also conducted, and rapid self-healing of the damaged printed objects is demonstrated.

## 2. Results and discussion

### 2.1. Synthesis of self-healing elastomers

Poly(2-[[(butylamino)carbonyl]oxy]ethyl acrylate) (Poly(BCOE)) is selected as the major polymer composition due to their weak and abundant hydrogen bonding, good thermal/chemical stability and sub-ambient glass-transition temperature ($T_g \sim -3$ °C) [13]. The low $T_g$ of the obtained elastomers is important to enable fast chain mobility and maintain self-healing performance. A monomer with quadruple H-bonds, i.e., 2-(3-(6-methyl-4-oxo-1,4-dihydropyrimidin-2-yl)ureido) ethyl methacrylate (MPA-UPy, Scheme 1), is synthesized for copolymerization with BCOE, and its chemical structure is confirmed by $^1$H nuclear magnetic resonance ($^1$H NMR) spectroscopy (Fig. S1a) [47]. As shown in Scheme 1, monomers with different H-bonding strengths, BCOE and MPA-UPy, are copolymerized at different molar ratios, i.e., 100:0, 99:1, 95:5, and 90:10. Herein, the ASCEs are distinguished by the molar percentages of MPA-UPy in the copolymer. For example, Poly (BCOE-*r*-UPy5) indicates that BCOE is copolymerized with MPA-UPy at a molar ratio of 95:5. Reversible addition−fragmentation chain-transfer (RAFT) polymerization technique was employed for polymer synthesis due to the advantages of delivering copolymers with consistent molecular weights as well as uniform and tunable compositions [48].

As illustrated by the $^1$H NMR spectrum (DMSO-d6 with presence of




**Scheme 1.** (a) Synthesis of room-temperature self-healable random copolymer Poly(BCOE-*r*-UPy)s. (b) Demonstration of the simplified structure and H-bonding interactions of Poly(BCOE-*r*-UPy). (c) Illustration of the self-healing process of Poly(BCOE-*r*-UPy).

$H_2O$ at 3.33 ppm) of Poly(BCOE-*r*-UPy5), the characteristic peaks d and j in Fig. 1a reveal the presence of both BCOE and MPA-UPy units, demonstrating a successful copolymerization process. The comparative integrations of peaks e and j are also utilized to determine the molar ratio of two monomer units in the obtained ASCE. As seen in Fig. 1a, the ratio between peak e and j is 100:5, comparable with the feed ratio between BCOE and MPA-UPy of 95:5. To calculate the molecular weight of Poly(BCOE-*r*-UPy)s, we compared the $^1$H NMR spectra of the Poly (BCOE-*r*-UPy1) reaction solution before and after the polymerization (Fig. S1c, d). The $^1$H NMR spectra indicates almost quantitative monomer conversion, thus, the theoretical calculation of molecular weights in Table S1 should reflect the actual molecular weights. The peak at 3388 $cm^{-1}$ in the attenuated total reflection Fourier-transform infrared (ATR-FTIR) spectra reflects the $N-H$ stretching in the polymer, and the peak between 3000 and 2840 $cm^{-1}$ is the characteristic peak of C—H stretching. The peak at 1665 $cm^{-1}$ is attributed to UPy's urea carbonyl group (Fig. 1c), while the peak at 1570 $cm^{-1}$ is associated with C–N–H bending and C–N stretching of the amide II (1470–1570 $cm^{-1}$) band [49, 50].

All of the Poly(BCOE-*r*-UPy) copolymers exhibit good thermal stability with less than 5 % weight loss until 230 °C, as illustrated by the thermogravimetric analysis (TGA) (see Fig. S1b). It is worth noting that the thermal stability of copolymers decreases slightly with an increased molar ratio of MPA-UPy, and the degradation temperature of Poly (BCOE-*r*-UPy10), which has the most UPy moiety among Poly(BCOE-*r*-UPy) copolymers, is comparable to the reported similar system [51]. As illustrated by the differential scanning calorimetry (DSC) data in Fig. 1b, all samples show a single glass transition temperature ($T_g$) ranging from −2.4 °C to 21.7 °C. Their low $T_g$ values indicate high chain mobility at ambient temperature, benefiting autonomous self-healing capability along with stretchability. A higher concentration of MPA-UPy units renders the increase of $T_g$ due to the higher density of quadruple H-bonds by UPy moieties that has significantly higher bond dissociation energy than typical H-bonding units (about 37.5 kJ $mol^{-1}$ for quadruple H-bonds in UPy *vs.* < 15 kJ $mol^{-1}$ for single hydrogen bonds) [52,53]. Meanwhile, there should be the contributions of H-bonding formed between the UPy and BCOE moiety [54]. The increase in $T_g$ is roughly proportional to the fraction of UPy units (Fig. 1b), in agreement with the predictions of recent theoretical work on the role of stickers in associating polymers [55]. Moreover, showing no peak in the SAXS data (Fig. 1d) indicates the absence of significant phase separation in all of the Poly(BCOE-*r*-UPy) samples [56]. This is consistent with the absence of a second $T_g$ in the DSC data (Fig. 1b).

### 2.2. Mechanical property evaluations

During the rheology tests, the storage modulus (G') and loss modulus (G") were measured with a frequency sweep applied to the samples. The master curves are obtained by combining the data at different temperatures using the temperature-frequency superposition (Fig. 2a) with the reference temperature of 298 K (25 °C). Without UPy units, the Poly (BCOE) exhibits a usual solid-like behavior with G' higher than G" at higher frequencies, whereas it exhibits liquid-like behavior with G' lower than G" at lower frequencies. With the incorporation of UPy moiety, G" and G' spectra shift to lower frequency due to slower segmental dynamics, and a rubbery plateau develops due to the appearance of temporal UPy crosslinks (Fig. 2a). The level of rubbery plateau $G'_r$ could be utilized to calculate the cross-link density *via* the following equation [57]

$$c_x = \frac{2G'_r}{3RT} = \frac{2\rho}{3M_x} \quad (1)$$

where $c_x$ is the moles of cross-links per volume (Fig. 2a), R is the gas

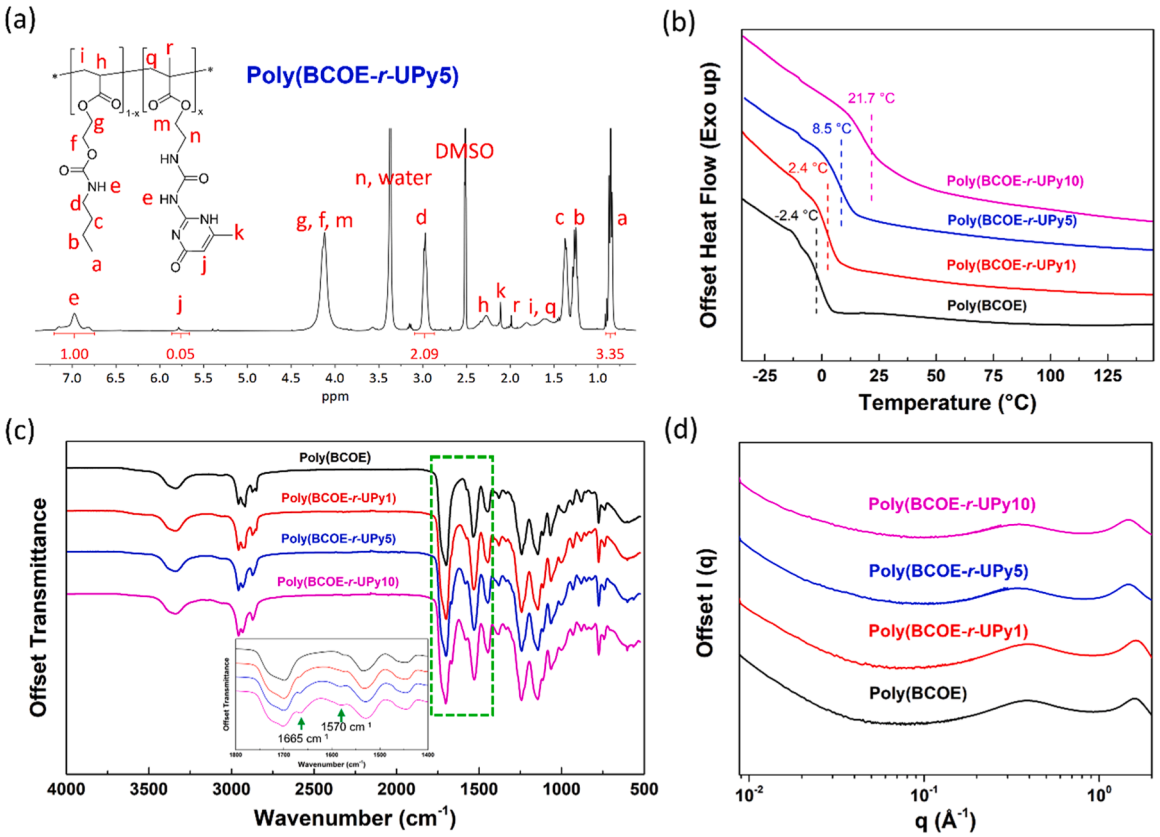



**Fig. 1.** (a) $^1$H NMR data of Poly(BCOE-*r*-UPy5). (b) DSC data of Poly(BCOE-*r*-UPy)s. (c) ATR-FTIR spectra of Poly(BCOE-*r*-UPy)s with different molar ratios of MPA-UPy. (d) Combined SAXS/WAXS spectra of Poly(BCOE) and Poly(BCOE-*r*-UPy)s with different molar ratios of MPA-UPy.

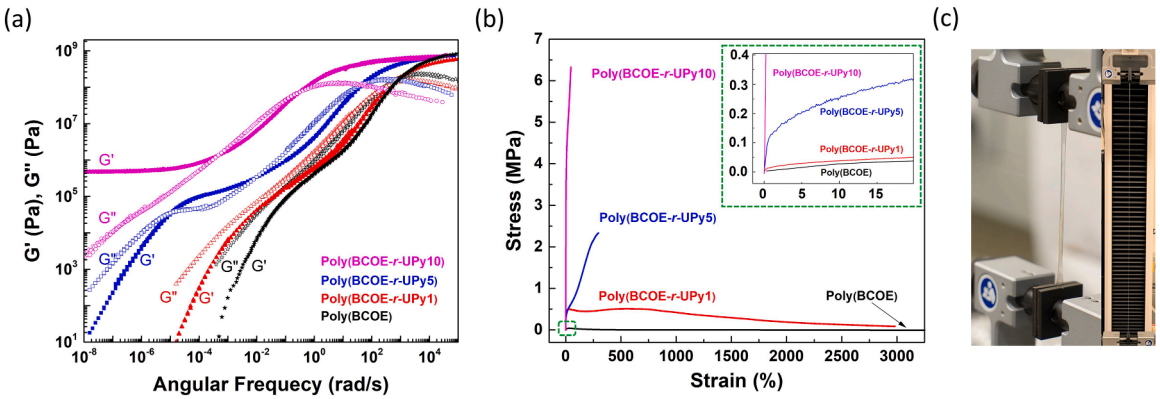



**Fig. 2.** (a) Storage modulus (G', closed symbols) and loss modulus (G", open symbols) (reference temperature = 25 °C) of Poly(BCOE) and Poly(BCOE-*r*-UPy)s. (b) Tensile data of Poly(BCOE) and Poly(BCOE-*r*-UPy)s with zoomed in regions. (c) Photo of Poly(BCOE) during tensile test (>3000% tensile strain).

constant, T is the temperature in Kelvin, ρ is polymer density, and $M_x$ is the number-average molecular weight between the cross-links. The calculated crosslink density $c_x$ and $M_x$ of Poly(BCOE-*r*-UPy5) and Poly (BCOE-*r*-UPy10) are listed in Table S1.

Tensile tests of Poly(BCOE-*r*-UPy)s were performed by testing the dog-bone-shaped specimens following the ASTM D1708 method. As seen in Fig. 2b, with an increase in MPA-UPy moiety ratio, the Poly (BCOE-*r*-UPy)s exhibit higher Young's modulus and ultimate tensile stress while reducing the elongation-at-break. Consistent with the rheology result, Poly(BCOE) is extremely soft and ductile with Young's modulus of only 300 Pa and elongation-at-break over 5000 %. With increased UPy fraction from 1 mol % to 10 mol%, Young's modulus of Poly(BCOE-*r*-UPy)s increases from 0.3 MPa to 33.2 MPa (Table 1). The increase in Young's modulus is contributed by the increase in crosslink density through more UPy units, and by slowing down of segmental relaxation (higher $T_g$, Table 1). Also, the reduced extensibility can be explained by the increased UPy moiety, rendering higher crosslink density with a slower bond rearrangement. Compared with H-bonding groups in BCOE units, the UPy bonds have higher resistance to dissociate and rearrangements due to their higher activation energy [58]. Thus, a trade-off between the ultimate tensile stress, Young's modulus, and elongation-at-break is observed for Poly(BCOE-*r*-UPy)s. For example, Poly(BCOE-*r*-UPy10) exhibits high rigidity and relatively low extensibility with Young's modulus of 33 MPa, and elongation-at-break of 49.6 %. We also observed the stress relaxation behavior of Poly(BCOE) and Poly(BCOE-*r*-UPy1) during the tensile test, which is expected in materials with reversible networks where the relaxation time is at the comparable time scale with the stretching process [59,60], When these samples exhibit high extensibility, the stretching time (> 150 s) matches their inherent stress relaxation time. The overall toughness of Poly (BCOE-*r*-UPy)s is not linearly related to the MPA-UPy ratio, and poly (BCOE-*r*-UPy1) exhibits the highest toughness of 9.0 MJ/$m^3$. The mechanical properties of Poly(BCOE-*r*-UPy)s could be well-tuned to satisfy different demands by simple control of their composition by tailoring the feed ratio of MPA-UPy over BCOE.

### 2.3. Self-healing performance

Since both BCOE and MPA-UPy units contain H-bonding and each individual component of the copolymer has been examined to possess self-healing properties [13,41,61], it is predictable that these polymers could undergo a self-healing process at certain conditions. During the mechanical testing, we observed that all samples showed some elastic recovery behavior during elongation process. The hysteresis data of Poly (BCOE-*r*-UPy5) also demonstrates 55 % of remaining tensile stress after 10 successive loading-unloading cycles (see Fig. S2). Considering the previous demonstration that cross-linked elastomer after local rupture could return to its initial equilibrium shape to facilitate self-healing process [62,63], we anticipate such elastic recovery behavior may also affect the self-healing properties of Poly(BCOE-*r*-UPy)s. The elastic recovery at ambient temperature is primarily contributed by the UPy moieties that introduce strong physical cross-links to the system, which is consistent with previous statement that stronger dynamic bonds is more responsible for elastic recovery at low strain values [64,65]. An optical microscope was first utilized to examine the healing capability of Poly(BCOE-*r*-UPy)s. As illustrated in Fig. 3a, the deep razor blade cut on Poly(BCOE-*r*-UPy1) sample was completely repaired after one day at room temperature (20 °C), demonstrating its rapid room-temperature self-healability. To compare the healing behavior between Poly(BCOE) and Poly(BCOE-*r*-UPy1), a razor blade was utilized to apply damage on the sample surfaces as shown in Fig. 3b. The razor blade cut on Poly (BCOE-*r*-UPy1) almost diminishes after 5-minute healing at 30 °C, while the scratch remains with smoothed edges for sample Poly(BCOE), indicating a superior healing efficiency of Poly(BCOE-*r*-UPy1).

Helium ion microscope (HIM) is an imaging technology utilizing a scanning helium ion beam [66,67], and herein, it is utilized to conduct the *in situ* observation of the self-healing process of Poly(BCOE-*r*-UPy1). As illustrated in Fig. 3c, a 15 μm × 30 μm cut was made by a razor blade on Poly(BCOE-*r*-UPy1) film, whose healing process is monitored continuously. The sample showed significant healing progress after 15 min, and the void disappeared completely in 60 min. The healing video assembled from multiple images is also attached in the supporting information. The utilization of HIM to continuously monitor the

**Table 1**
Combined physical properties of Poly(BCOE) and Poly(BCOE-*r*-UPy)s.

| Sample | $T_{d,\ 5\ \%}$ (°C) | $T_g$ (°C) | Density (g/$cm^3$) | Young's modulus (MPa) | Elongation-at-break (%) | Ultimate Tensile Strength (MPa) | Toughness (MJ/$m^3$) |
|---|---|---|---|---|---|---|---|
| **Poly(BCOE)** | 260.1 | −2.4 | 1.156 | $2.7 \times 10^{-4}$ | > 5000 | 0.04 | 0.07 |
| **Poly(BCOE-*r*-UPy1)** | 258.2 | 2.4 | 1.156 | 0.3 ± 0.01 | 2871.3 ± 193.4 | 0.5 ± 0.02 | 9.0 ± 0.4 |
| **Poly(BCOE-*r*-UPy5)** | 233.3 | 8.5 | 1.191 | 1.6 ± 0.1 | 232.6 ± 11.1 | 2.6 ± 0.08 | 2.8 ± 0.3 |
| **Poly(BCOE-*r*-UPy10)** | 239.2 | 21.7 | 1.207 | 33.2 ± 2.1 | 49.6 ± 4.2 | 6.3 ± 0.03 | 2.4 ± 0.1 |

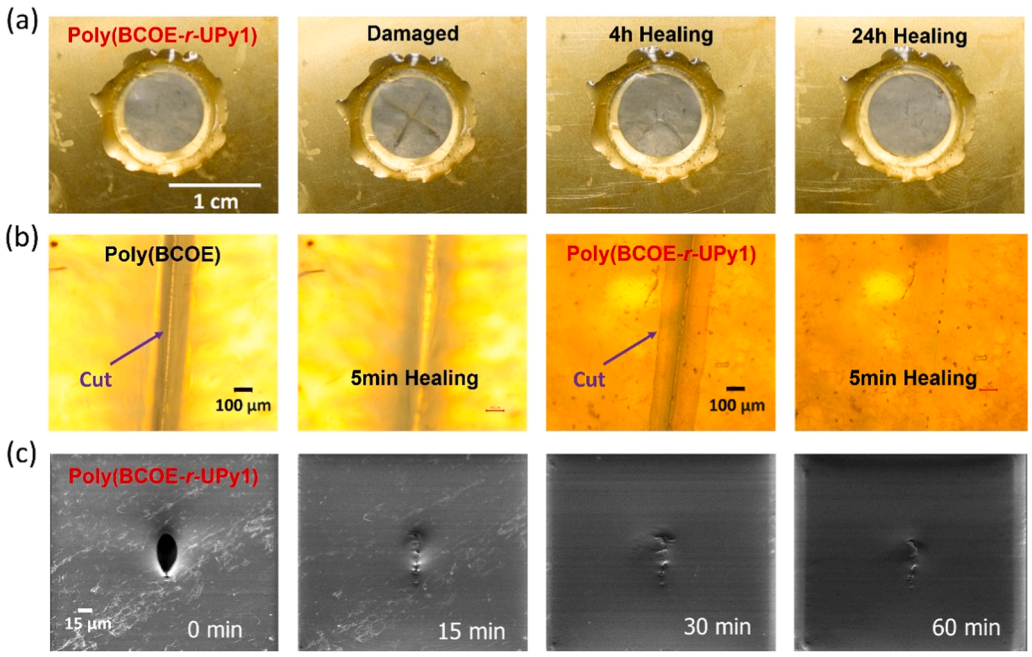



**Fig. 3.** (a) Photograph of damaged and healed (4 h, 24 h) Poly(BCOE-*r*-UPy1) sample at 20 °C. (b) Optical microscope images demonstrating the healing process of Poly(BCOE) and Poly(BCOE-*r*-UPy1) against cut by a razor blade. (c) Helium-ion microscope images, demonstrating the healing process of Poly(BCOE-*r*-UPy1) against cut by a razor blade.

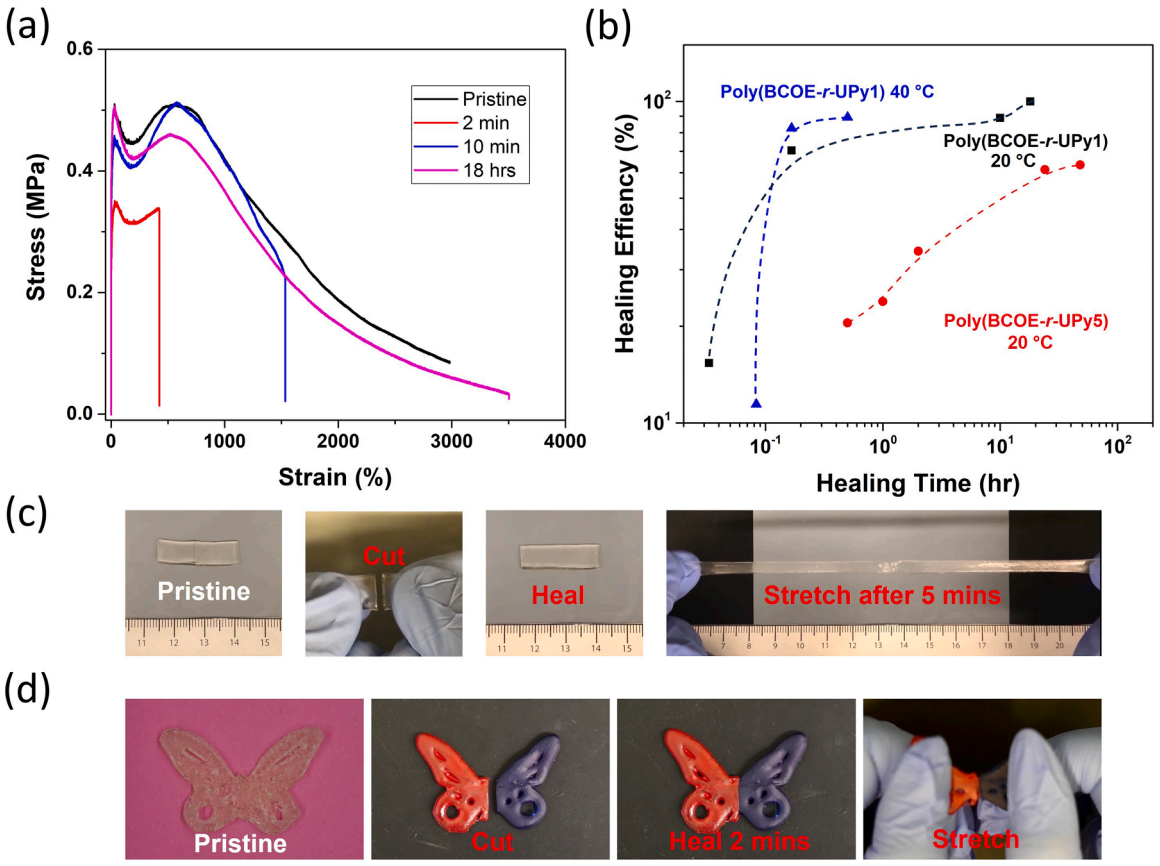



**Fig. 4.** (a) Tensile data of Poly(BCOE-*r*-UPy1) and cut sample with different healing time. (b) Healing efficiency of Poly(BCOE-*r*-UPy1) different healing temperatures and times, Poly(BCOE-*r*-UPy5) at different healing times. (c) Photo demonstration of self-healability of Poly(BCOE-*r*-UPy1) at room temperature. (d) Pictures showing the healing process of 3D-printed Poly(BCOE-*r*-UPy5) sample.

self-healing process of elastic polymers at the micro-scale provided high-resolution tracking. Overall, Poly(BCOE-*r*-UPy1) is self-healable towards physical scratch with a scale from 15 μm to 1 cm within 15 min at ambient temperature.

Quantitative analysis of self-healing kinetics is conducted by comparing the tensile properties between the pristine sample and healed sample at different healing times. The mechanical properties evaluations were all performed at ambient temperature for fair comparison even for those examples healed at elevated temperatures [31,68]. At room temperature, 18 h is required to obtain fully recovered mechanical properties, including Young's modulus, elongation-at-break, ultimate tensile strength, and toughness (see Fig. 4a). The self-healing kinetics of Poly (BCOE-*r*-UPy1) and Poly(BCOE-*r*-UPy5) are studied by calculating their comparative toughness with pristine samples, and a recovery percentage is obtained for each sample at different healing times (see Fig. 4b). Poly (BCOE-*r*-UPy1) outperforms Poly(BCOE-*r*-UPy5) in terms of the healing efficiency at 20 °C: Poly(BCOE-*r*-UPy1) achieves more than 95 % healing efficiency after 18 h, while Poly(BCOE-*r*-UPy5) achieves only 60 % healing efficiency with the same time length. With much higher activation energy than single H-bonding units [58], UPy crosslinks require more energy and time to dissociate and rearrange. We also examined the self-healing properties of Poly(BCOE-*r*-UPy1) at 40 °C to unravel the healing properties at elevated temperatures. We discovered that Poly (BCOE-*r*-UPy1) recovered nearly 90 % of its original toughness after 30 mins of healing (Fig. S3), which has been significantly accelerated by faster segmental dynamics and UPy-bonds rearrangements. We noticed that although over 90 % of the toughness was recovered after 30 mins of healing, the tensile strength and modulus were not fully recovered, because of that while the healing was conducted at 40 °C, the tensile testing was still conducted at 20 °C immediately after healing due to instrumental limitation, and thus, the residual heat introduced a softening effect to the mechanical properties.

The sample with a higher concentration of UPy contents such as Poly (BCOE-*r*-UPy5) requires more time for mechanical recovery. Moreover, due to higher $T_g$, the segmental dynamics of Poly(BCOE-*r*-UPy5) at RT are significantly slower than that of Poly(BCOE-*r*-UPy1), also contributing to a slower self-healing rate at room temperature. Another aspect to interpret the self-healing behavior is to compare their flowability. As seen in Fig. 2a, the terminal relaxation time differs ~1000 times between UPy1 and UPy5 systems, indicating a significantly higher flowability of Poly(BCOE-*r*-UPy1). At 20 °C, the Poly(BCOE-*r*-UPy1) exhibits superior self-healing performance than Poly(BCOE-*r*-UPy5) and Poly (BCOE-*r*-UPy10), because Poly(BCOE-*r*-UPy1) is below the gel point, while the Poly(BCOE-*r*-UPy5) and Poly(BCOE-*r*-UPy10) are above the gel point. The high flowability of Poly(BCOE-*r*-UPy1) enables such room-temperature self-healing performance. For Poly(BCOE-*r*-UPy5) and poly(BCOE-*r*-UPy10), since the polymer segments could not move sufficiently, they do not self-heal well at 20 °C. Higher flowability of the polymer has significant impact on the self-healing kinetics (Fig. 4b). Therefore, 70 % recovery in Poly(BCOE-*r*-UPy1) is achieved and ~500 times faster than in Poly(BCOE-*r*-UPy5), which agrees with the comparative terminal relaxation time of these samples (~ 3 orders difference, Fig. 2a). Aside from flowability of polymer chain, construction of efficient supramolecular network *via* addition of UPy moiety is also vital for self-healability considering the fact that the Poly(BCOE-*r*-UPy1) shows superior self-healability than Poly(BCOE) [69]. The self-dimerization of UPy occurs easily with a dimerization constant up to the level of $10^7$ $M^{-1}$ [58,70,71]. Such high association constant facilitates the healing process [54,72]. By tuning the moiety ratio of UPy moieties that affects $T_g$, we obtained the samples with balanced self-healing ability and mechanical performance, i.e., Poly(BCOE-*r*--UPy1) and Poly(BCOE-*r*-UPy5).

The toughness recovery (%) against time (min) of Poly(BCOE-*r*-UPy1) is compared with other reported self-healable polymers based on H-bonds (Fig. 5) [31,33,35,43,68,73]. For example, Leibler and coworkers developed a self-healing elastomer with room-temperature healability, and it recovered 5.3 % of original toughness in 15 min of healing and achieved almost full recovery after 3-hour healing [31]. Our Poly(BCOE-*r*-UPy1) exhibits exceptionally fast self-healing capability with more than 70 % toughness recovery in 10 min, outperforming a series of recently reported H-bonding facilitated self-healable polymers that typically require 4–24 h for 70 % of toughness recovery at room temperature. This suggests that, in terms of healing efficiency, Poly (BCOE-*r*-UPy1) is one of the fastest H-bonding facilitated autonomous self-healable polymers. We also compared the healing properties of Poly (BCOE-*r*-UPy)s with other healable polymers in a log–log plot with over 90 % of mechanical recovery [16]. As illustrated in Fig. 5b, Poly (BCOE-*r*-UPy1) exhibits a good balance between the tensile strength and healing rate, which is comparable or superior to other state-of-the-art (blue trend line) self-healing materials. As illustrated by the underwater test in Fig. S7, the cut Poly(BCOE-*r*-UPy1) sample can also be healed underwater, where 30 min healing was sufficient for hand stretching the sample despite being cut.

Additive manufacturing (AM) is an emerging technique due to its multiple advantages over traditional subtractive manufacturing such as computer numerical control (CNC) machining, customized on-demand manufacturing in a rapid manner from the design to finish as well as less waste. One of the most developed AM techniques is fused deposition modeling (FDM), where thermoplastics such as acrylonitrile butadiene styrene (ABS) and polylactic acid (PLA) are melted and extruded to

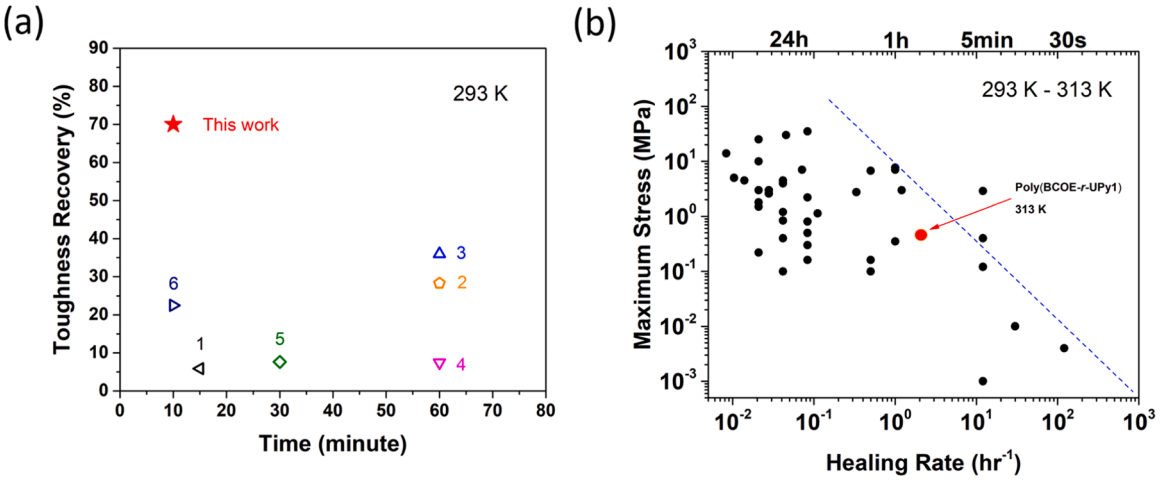



**Fig. 5.** (a) Comparison of the toughness recovery percentage and healing time of the Poly(BCOE-*r*-UPy1) with recently reported self-healable polymers. (1, ref. [31]; 2, ref. [68]; 3, ref. [43]; 4, ref. [33]; 5, ref. [35]; 6, ref. [73]). (b) Healing properties of Poly(BCOE-*r*-UPy1) at 313 K compared with other self-healing polymers[16].

obtain target objects [74]. AM of dynamically crosslinked polymers is an emerging concept due to their mechanical robustness, solvent resistance, good recyclability, and self-healability [75–78]. To investigate the potentials on printing a self-healable 3D object, we utilized Poly (BCOE-*r*-UPy5) for AM due to its good mechanical strength (ultimate tensile strength, 2.55 MPa) as well as high extensibility (strain, 232 %) and flow behavior at high temperature. As shown in Fig. 4d, an AM process is demonstrated with a butterfly-shaped product on the surface in a commercially available 3D printer. The completely cut sample exhibits a self-healing character after a 5-minute healing process at room temperature. The printing result indicates that the Poly(BCOE-*r*-UPy5) fits the criteria of FDM feed materials, which can be utilized in multiple 3D printing scenarios. The demonstration of FDM on readily self-healable elastomers sheds light on custom-designed intricate 3D objects possessing self-healing capability. With the characteristics demonstrated above, we anticipate this Poly(BCOE-*r*-UPy) copolymer could be well utilized as a sealant against water leakage, as it fits the criteria of room-temperature healability and fast mechanical recovery. A demonstration of such capabilities is shown in Fig. S5, the Poly (BCOE-*r*-UPy1) sample healed for only 5 mins and exhibited similar sealing and protecting nature against the water droplet as the pristine sample.

### 2.4. Dynamic studies for self-healing mechanism

The self-healing process is enabled by the formation of a bridge through reversible dynamic bonds across the interface of fracture, and such a process requires the transient network rearrangement with timescale controlled by the bond dissociation energy. Thus, it is of paramount importance to estimate and understand microscopic dynamics, i.e., how dynamic bond dissociation and its energy barrier result in the network rearrangement. When estimating bond dissociation energy, it is imperative to consider the segmental dynamics which provides the prerequisite for bond rearrangement [79,80]. Thus, broadband dielectric spectroscopy (BDS) was employed to study the segmental dynamics of the Poly(BCOE-*r*-UPy5) as an example. Only one relaxation process was observed in the dielectric loss ($\varepsilon''$) spectra, followed by the conductivity contribution at lower frequencies (Fig. 6a). The fitting method is described in SI. The eq. S1 describes the spectra well, and example of the fit of $\varepsilon''$ spectra is shown in Fig. S4. The so obtained $\tau_{max}(T)$ was fit to the VFT equation,

$$\tau_{max}(T) = \tau_0 \exp\left(\frac{B}{T - T_0}\right) \quad (2)$$

in which $\tau_0$, $B$ and $T_0$ are 3 free fit parameters. The temperature at which extrapolated $\tau_{max}(T)$ reaches 100 s, agrees well with $T_g$ measured by DSC, indicating that the measured dielectric process results from the segmental motion, i.e., α relaxation process.

The terminal relaxation time ($\tau_C$) indicating network rearrangement is acquired from the crossover of G' and G" in the master curve of shear modulus (Fig. 2a). The temperature dependence of $\tau_C(T)$ was acquired in the limited temperature range when the crossover was in the measurable frequency window, still using time-temperature superposition (TTS) for higher accuracy. To estimate the bond dissociation energy, $\tau_C(T)$ was analyzed through the following equation by considering segmental $\tau_\alpha$(T) as a pre-factor [81]:

$$\tau_C(T) = \tau_\alpha(\mathrm{T})\exp\left(\frac{E_a}{RT}\right) = \tau_0 \exp\left(\frac{B}{T - T_0} + \frac{E_a}{RT}\right) \quad (3)$$

In the fitting, $\tau_0$, $B$, $T_0$ were fixed based on the VFT fitting of the segmental relaxation (Fig. 6b), and $E_a$, the activation energy, was the only free fit parameter. The fit to the eq. (3) describes $\tau_C(T)$ well (Fig. 6b), indicating that both the segmental dynamic and the energy barrier from transient bond dissociation contribute to the bond dissociation process. The activation energy $E_a$ was estimated at ~ 37.5 kJ/mol, which is a typical dissociation energy for UPy functional groups and roughly corresponds to the dissociation energy of four H-bonds.

## 3. Conclusions

A series of self-healing polymers, Poly(BCOE-*r*-UPy)s are developed by copolymerization of controlled ratios between BCOE and MPA-UPy monomer by RAFT polymerization. Tuning the ratio between the two different monomers in Poly(BCOE-*r*-UPy)s provides varied H-bonding forces and allows good control of the mechanical properties and self-healing capabilities. Both segmental dynamic and energy barrier from transient bond dissociation contribute to the bond dissociation process. The hydrogen-bonding units provide temporary crosslinks with characteristic dissociation energy ~37.5 kJ/mol, which is calculated from the temperature dependence of terminal relaxation $\tau_C$ (from the crossover of G' and G" in the master curve of shear modulus), followed by subtracting the segmental relaxation $\tau_\alpha$ (obtained from BDS). Adjusting the $T_g$ of copolymers through controlled concentration of UPy units leads to Poly(BCOE-*r*-UPy)s with high chain mobility, which significantly improves the self-healing capability. In situ microscopy analysis by HIM confirmed the 15-min healability of Poly(BCOE-*r*-UPy) at a scale of 15 μm. The self-healing kinetics of Poly(BCOE-*r*-UPy)s are studied by calculating their toughness recovery in comparison to the pristine samples. The Poly(BCOE-*r*-UPy1) sample achieves an overall

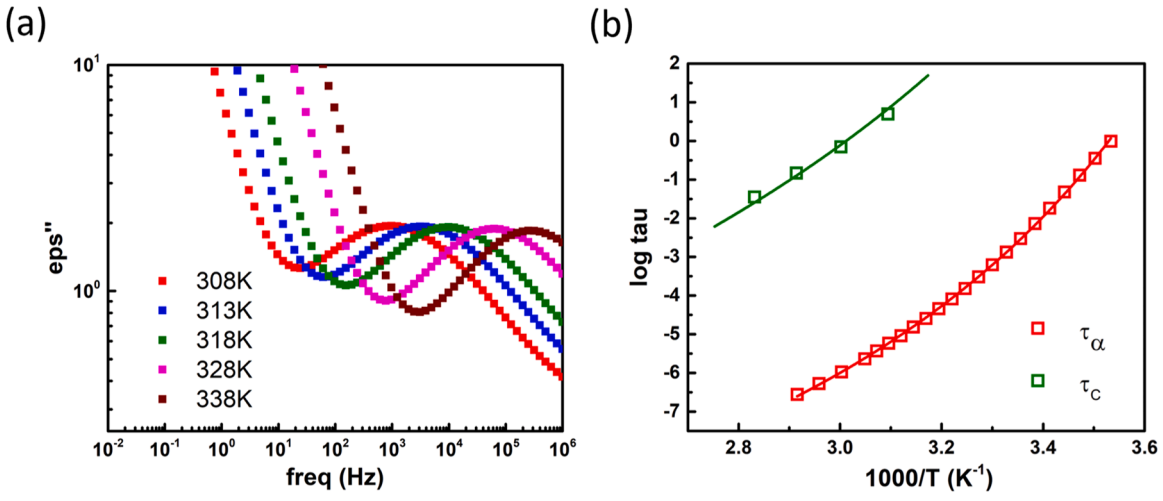



**Fig. 6.** (a) $\varepsilon_{der}$ for Poly(BCOE-*r*-UPy5). (b) Activation plot of Poly(BCOE-*r*-UPy5) with $\tau_\alpha$and $\tau_C$.

mechanical toughness recovery of 70 % within 10 min of healing process, superior to the reported H-bonding facilitated self-healable polymers. The 3D printing capability of Poly(BCOE-*r*-UPy5) was also demonstrated, and the 3D printed object could undergo a room-temperature self-healing process.

The combination of different types of H-bonding units to facilitate self-healing is demonstrated to be a practical pathway to fabricate self-healable polymers with controllable properties. An insight into the structure-property relationship is delivered with rational physical analysis, which will provide important guidance for analyzing the dynamics of self-healing materials. The fast, room-temperature self-healable, 3D-printable Poly(BCOE-*r*-UPy)s exhibit important design parameters for future fabrication of functional membranes, sealants, coatings, and devices with repairable properties.

## 4. Experimental

### 4.1. Materials

All reagents were obtained from Sigma Aldrich and were used as received, except for BCOE, which was purified through inhibitor remover and basic $Al_2O_3$ columns.

### 4.2. Synthesis of MPA-UPy

A flame-dried 100 mL round bottom flask with a magnetic stir bar was utilized, 54.80 g (0.35 mol) of 2-isocyanatoethyl methacrylate (contains $\leq$ 0.1 % BHT as inhibitor), 40.18 g (0.32 mol) of 2-amino-4-hydroxy-6-methylpyrimidine, and 30 mL of anhydrous dimethyl sulfoxide were added into the flask. The round bottom flask was sealed by a rubber stopper and was purged with continuous $N_2$ flow during the reaction. The flask was submerged into a 140 °C oil bath for 25 min. After the reaction was completed, 100 mL of methanol was added into the flask, white solid-like precipitants were obtained. The white solid was collected and washed by 50 mL of methanol three times. The final product was obtained and dried under vacuum at 85 °C to remove all solvents.

### 4.3. Synthesis of the poly(BCOE-r-UPy) polymer

The inhibitors in the 2-[[(Butylamino)carbonyl]oxy]ethyl acrylate monomer was removed by passing the monomer through a basic $Al_2O_3$/inhibitor remover mixed column prior to the polymerization. Detailed synthesis procedures of Poly(BCOE-*r*-UPy1) is shown below as example: a flame-dried 100 mL Schlenk tube with a magnetic stir bar was utilized, 44.75 mg (0.188 mmol) 2-(Butylthiocarbonothioylthio)propanoic acid, 10.0 g (46.46 mmol) of 2-[[(Butylamino)carbonyl]oxy]ethyl acrylate, 131.73 mg (0.47 mmol) of MPA-UPy, and 7.70 mg (0.047 mmol) of recrystallized azobisisobutyronitrile were added into the tube followed by 30 mL of anhydrous dimethylformamide (DMF). The tube was sealed by a rubber stopper and $N_2$ was purged for 30 mins to remove the air inside the tube. Then, under continuous $N_2$ flow, the tube was submerged in a 65 °C oil bath for 24 h. After the reaction was completed, the polymer was precipitated into 300 mL of water in a 500 mL beaker under stirring. The yellow solid was collected and dissolved by 50 mL of ethyl acetate. Then the solution was precipitated into 300 mL of diethyl ether, this procedure was repeated for an additional cycle. After the complete removal of monomers by dialysis, the final product was obtained and dried under vacuum at 85 °C to remove all solvents.

### 4.4. Molecular structure and thermal analysis

$^1$H Nuclear magnetic resonance (NMR) spectra were recorded on a Bruker 400 MHz NMR spectrometer using $CDCl_3$. Infrared (IR) spectra were obtained from a Nicolet iS50 FT-IR spectrometer (Thermo Scientific), and the scanning range was 4000 - 400 $cm^{-1}$. Approximately 10 mg of each sample was weighted out to test on TGA Q50, TA Instrument. The samples were heated up to 800 °C from room-temperature at a heating rate of 20 °C/ min under a dry nitrogen atmosphere (flow rate: 40 mL/min). Thermal transitions of polymers were studied using modulated DSC (TA DSC 2500). The heating procedure was set to modulate +/- 1.00 °C every 60 s at the rate of 3 °C/min from − 30 to 150 °C.

### 4.5. Tensile and rheology analysis

Rectangular stripes were prepared by melt-press at 50 °C, and films were cut into approximately (7.0 × 5.0 × 0.5) mm specimens for tensile analysis using an Instron 3343 Universal Testing System with a 50 N load cell. Samples were elongated at the rate of 1 mm/s till break. The reported tensile properties were an average of a minimum of three samples. Hysteresis tests were conducted on a TA instrument DMA850 with similar sample specimens above. The sample was first elongated to 100 % strain and then compressed to 0 % strain at the same rate, 10 cycles were performed at the rate of 1 mm/s under ambient conditions.

Small-amplitude oscillatory shear (SAOS) measurements of membrane samples were carried out on an AR2000ex rheometer (TA Instruments) with an angular frequency range from $10^{-1}$ to $10^2$ rad/s using parallel plate geometry with a disk diameter of 4 mm. The temperature was controlled by an environmental test chamber filled with nitrogen. Prior to measurements, the sample was purged at 80 °C for 0.5 h under a nitrogen atmosphere to ensure thermal equilibrium was achieved. The samples were measured at a variety of temperatures ranging from $T_g$ to 100 °C. The strain amplitude during the measurement was chosen to be in the range from 0.03 % to 5 % depending on the modulus level at different temperatures.

### 4.6. Dielectric measurement

Broadband Dielectric Spectroscopy (BDS) in the frequency range from $10^{-2}$ to $10^6$ Hz were measured utilizing a Novocontrol system that includes an Alpha-A impedance analyzer and a Quatro Cryosystem temperature control unit. All samples were placed into a parallel plate dielectric cell made of sapphire and invar steel with an electrode diameter of 10 mm, and capacitance 3.3 pF with an electrode separation of 210 μm. The measurement started 10 K below the $T_g$. All the spectra were measured on heating. After each temperature increase, the samples were equilibrated for 10 min to reach thermal stabilization within 0.1 K.

The $\varepsilon''$ spectra were fit using one Havriliak-Ngami (HN) function plus conductivity, i.e.,

$$\varepsilon''(\upsilon) = -Im\left\{\frac{\Delta\varepsilon}{[1+(2\pi i\upsilon\tau)^{\alpha}]^{\gamma}}\right\} + \frac{\sigma}{2\pi\upsilon\varepsilon_0} \tag{4}$$

Here $\Delta\varepsilon$ denotes the dielectric strength and $\alpha$ and $\gamma$ are the shape parameters. $\varepsilon_0$ indicates the vacuum permittivity, σ indicates the conductivity, and $\tau$ is HN relaxation time which is related to the relaxation time at the loss maximum ($\tau_{max}$):

$$\tau_{max} = \tau\left[\sin\left(\frac{\alpha\pi}{2+2\gamma}\right)\right]^{-\frac{1}{\alpha}}\left[\sin\left(\frac{\alpha\gamma\pi}{2+2\gamma}\right)\right]^{\frac{1}{\alpha}} \tag{5}$$

$\tau_{max}$ is widely used as the characteristic relaxation time in polymeric materials.

## Supplementary information

Supporting Information includes experimental details, $^1$H NMR spectrum, TGA, tensile, and BDS data.

## Declaration of Competing Interest

The authors declare that they have no known competing financial

interests or personal relationships that could have appeared to influence the work reported in this paper.

## Acknowledgement

This study was supported by the U.S.-China Clean Energy Research Center for Building Energy Efficiency (CERC BEE) under the Building Technologies Office (BTO) of the U.S. Department of Energy (DOE) during the initial preparation and revision of the manuscript. The research was also supported by the Natural Science Foundation of China (52373275) during the rewriting and revision of the manuscript. The mechanical analysis, manufacturing, and healing kinetic study were supported by the U.S. DOE, Office of Science, Basic Energy Sciences, Materials Sciences and Engineering Division. NSF Polymer program (award DMR-1904657) supported the dielectric measurements and data analysis. A portion of this research was conducted at the Center for Nanophase Materials Sciences, which is a DOE Office of Science User Facility. The authors acknowledge Jackie Zheng and Shengyi Su for their help during the synthesis and testing of the materials.

## Supplementary materials

Supplementary material associated with this article can be found, in the online version, at doi:10.1016/j.supmat.2023.100042.

## References

[1] X. Wang, Y. Li, Y. Qian, H. Qi, J. Li, J. Sun, Mechanically robust atomic oxygen-resistant coatings capable of autonomously healing damage in low earth orbit space environment, Adv. Mater. 3036 (2018), 1803854.
[2] Q. Wang, W. Wang, X. Ji, X. Hao, C. Ma, W. Hao, X. Li, S. Chen, Self-healing coatings containing core–shell nanofibers with ph-responsive performance, ACS Appl. Mater. Interfaces 132 (2021) 3139–3152.
[3] H. Qian, D. Xu, C. Du, D. Zhang, X. Li, L. Huang, L. Deng, Y. Tu, J.M.C. Mol, H. A. Terryn, Dual-action smart coatings with a self-healing superhydrophobic surface and anti-corrosion properties, J. Mater. Chem. A 55 (2017) 2355–2364.
[4] C. Wang, H. Wu, Z. Chen, M.T. McDowell, Y. Cui, Z. Bao, Self-healing chemistry enables the stable operation of silicon microparticle anodes for high-energy lithium-ion batteries, Nat. Chem. 512 (2013) 1042–1048.
[5] H.J. Sim, H. Kim, Y. Jang, G.M. Spinks, S. Gambhir, D.L. Officer, G.G. Wallace, S. J. Kim, Self-Healing Electrode with High Electrical Conductivity and Mechanical Strength for Artificial Electronic Skin, ACS Appl. Mater. Interfaces 1149 (2019) 46026–46033.
[6] S. Liu, S. Chen, W. Shi, Z. Peng, K. Luo, S. Xing, J. Li, Z. Liu, L. Liu, Self-healing, robust, and stretchable electrode by direct printing on dynamic polyurea surface at slightly elevated temperature, Adv. Funct. Mater. 3126 (2021), 2102225.
[7] H. Guo, Y.J. Tan, G. Chen, Z. Wang, G.J. Susanto, H.H. See, Z. Yang, Z.W. Lim, L. Yang, B.C.K. Tee, Artificially innervated self-healing foams as synthetic piezo-impedance sensor skins, Nat. Commun. 111 (2020) 5747.
[8] J. Xu, Z. Guo, Y. Chen, Y. Luo, S. Xie, Y. Zhang, H. Tan, L. Xu, J. Zheng, Tough, adhesive, self-healing, fully physical crosslinked κ-CG-K+/pHEAA double-network ionic conductive hydrogels for wearable sensors, Polymer 236 (2021), 124321.
[9] H. Bai, Y.S. Kim, R.F. Shepherd, Autonomous self-healing optical sensors for damage intelligent soft-bodied systems, Sci. Adv. 849 (2022) eabq2104.
[10] P.-F. Cao, B. Li, T. Hong, J. Townsend, Z. Qiang, K. Xing, K.D. Vogiatzis, Y. Wang, J.W. Mays, A.P. Sokolov, T. Saito, Superstretchable, self-healing polymeric elastomers with tunable properties, Adv. Funct. Mater. 2822 (2018), 1800741.
[11] F. Ramos-Saz, C.S.M. Kang, M. Forsyth, J.M. Pringle, Highly selective and tunable co2/n2 separation performance in ammonium-based organic ionic plastic crystal composite membranes with self-healing properties, ACS Appl. Polym. Mater. 42 (2022) 1487–1496.
[12] D.-P. Wang, Z.-H. Zhao, C.-H. Li, J.-L. Zuo, An ultrafast self-healing polydimethylsiloxane elastomer with persistent sealing performance, Mater. Chem. Front. 37 (2019) 1411–1421.
[13] Z. Zhang, N. Ghezawi, B. Li, S. Ge, S. Zhao, T. Saito, D. Hun, P.-F. Cao, Autonomous self-healing elastomers with unprecedented adhesion force, Adv. Funct. Mater. 314 (2021), 2006298.
[14] M.Z. Rong, M.Q. Zhang, W. Zhang, A novel self-healing epoxy system with microencapsulated epoxy and imidazole curing agent, Adv. Compos. Lett. 165 (2007), 096369350701600502.
[15] K. Biswas, D. Gilmer, N. Ghezawi, P.-F. Cao, T. Saito, Demonstration of self-healing barrier films for vacuum insulation panels, Vacuum 164 (2019) 132–139.
[16] B. Li, P.-F. Cao, T. Saito, A.P. Sokolov, Intrinsically self-healing polymers: from mechanistic insight to current challenges, Chem. Rev. 1232 (2023) 701–735.
[17] G. Thangavel, M.W.M. Tan, P.S. Lee, Advances in self-healing supramolecular soft materials and nanocomposites, Nano Converg. 61 (2019) 29.
[18] H. Wang, H. Liu, Z. Cao, W. Li, X. Huang, Y. Zhu, F. Ling, H. Xu, Q. Wu, Y. Peng, B. Yang, R. Zhang, O. Kessler, G. Huang, J. Wu, Room-temperature autonomous self-healing glassy polymers with hyperbranched structure, Proc. Natl. Acad. Sci. U.S.A. 11721 (2020) 11299–11305.
[19] S. Zechel, R. Geitner, M. Abend, M. Siegmann, M. Enke, N. Kuhl, M. Klein, J. Vitz, S. Gräfe, B. Dietzek, M. Schmitt, J. Popp, U.S. Schubert, M.D. Hager, Intrinsic self-healing polymers with a high E-modulus based on dynamic reversible urea bonds, NPG Asia Mater. 98 (2017) e420. -e420.
[20] B. Willocq, J. Odent, P. Dubois, J.-M. Raquez, Advances in intrinsic self-healing polyurethanes and related composites, RSC Adv. 1023 (2020) 13766–13782.
[21] J. Zhao, Z. Zhang, C. Wang, X. Yan, Synergistic dual dynamic bonds in covalent adaptable networks, CCS Chem. 00 (2023) 1–16.
[22] Y.-L. Liu, T.-W. Chuo, Self-healing polymers based on thermally reversible diels–alder chemistry, Polym. Chem. 47 (2013) 2194–2205.
[23] M.B. Larsen, A.J. Boydston, "Flex-Activated" Mechanophores: using polymer mechanochemistry to direct bond bending activation, J. Am. Chem. Soc. 13522 (2013) 8189–8192.
[24] J. Canadell, H. Goossens, B. Klumperman, Self-healing materials based on disulfide links, Macromolecules 448 (2011) 2536–2541.
[25] J. Zhu, S. Zhao, J. Luo, W. Niu, T. Damron Joshua, Z. Zhang, A. Rahman Md, A. Arnould Mark, T. Saito, R. Advincula, P. Sokolov Alexei, G. Sumpter Bobby, P.-F. Cao, A novel dynamic polymer synthesis via chlorinated solvent quenched depolymerization, CCS Chem. 00 (2022) 1–13.
[26] J.J. Cash, T. Kubo, A.P. Bapat, B.S. Sumerlin, Room-Temperature Self-Healing Polymers Based on Dynamic-Covalent Boronic Esters, Macromolecules 487 (2015) 2098–2106.
[27] M. Burnworth, L. Tang, J.R. Kumpfer, A.J. Duncan, F.L. Beyer, G.L. Fiore, S. J. Rowan, C. Weder, Optically healable supramolecular polymers, Nature 4727343 (2011) 334–337.
[28] S. Yu, H. Zuo, X. Xu, N. Ning, B. Yu, L. Zhang, M. Tian, Self-healable silicone elastomer based on the synergistic effect of the coordination and ionic bonds, ACS Appl. Polym. Mater. 35 (2021) 2667–2677.
[29] F. Ding, H. Ding, Z. Shen, L. Qian, J. Ouyang, S. Zeng, T.A.P. Seery, J. Li, G. Wu, S. E. Chavez, A.T. Smith, L. Liu, Y. Li, L. Sun, Super Stretchable and Compressible Hydrogels Inspired by Hook-and-Loop Fasteners, Langmuir 3725 (2021) 7760–7770.
[30] B. Fan, N. Cui, Z. Xu, K. Chen, P. Yin, K. Yue, W. Tang, Thermoresponsive and self-healing hydrogel based on chitosan derivatives and polyoxometalate as an antibacterial coating, Biomacromolecules 223 (2022) 972–982.
[31] P. Cordier, F. Tournilhac, C. Soulié-Ziakovic, L. Leibler, Self-healing and thermoreversible rubber from supramolecular assembly, Nature 4517181 (2008) 977–980.
[32] W. Wang, S. Wang, R. Rastak, Y. Ochiai, S. Niu, Y. Jiang, P.K. Arunachala, Y. Zheng, J. Xu, N. Matsuhisa, X. Yan, S.-K. Kwon, M. Miyakawa, Z. Zhang, R. Ning, A.M. Foudeh, Y. Yun, C. Linder, J.B.H. Tok, Z. Bao, Strain-insensitive intrinsically stretchable transistors and circuits, Nat. Electron. 42 (2021) 143–150.
[33] T. Yuan, X. Qu, X. Cui, J. Sun, Self-healing and recyclable hydrogels reinforced with in situ-formed organic nanofibrils exhibit simultaneously enhanced mechanical strength and stretchability, ACS Appl. Mater. Interfaces 1135 (2019) 32346–32353.
[34] B.C.K. Tee, C. Wang, R. Allen, Z. Bao, An electrically and mechanically self-healing composite with pressure- and flexion-sensitive properties for electronic skin applications, Nat. Nanotechnol. 712 (2012) 825–832.
[35] Z. Xu, L. Chen, L. Lu, R. Du, W. Ma, Y. Cai, X. An, H. Wu, Q. Luo, Q. Xu, Q. Zhang, X. Jia, A Highly-adhesive and self-healing elastomer for bio-interfacial electrode, Adv. Funct. Mater. 311 (2021), 2006432.
[36] T.-P. Huynh, H. Haick, Self-healing, fully functional, and multiparametric flexible sensing platform, Adv. Mater. 281 (2016) 138–143.
[37] D. Zhang, Y. Tang, Y. Zhang, F. Yang, Y. Liu, X. Wang, J. Yang, X. Gong, J. Zheng, Highly stretchable, self-adhesive, biocompatible, conductive hydrogels as fully polymeric strain sensors, J. Mater. Chem. A 839 (2020) 20474–20485.
[38] S. Banerjee, R. Tripathy, D. Cozzens, T. Nagy, S. Keki, M. Zsuga, R. Faust, Photoinduced smart, self-healing polymer sealant for photovoltaics, ACS Appl. Mater. Interfaces 73 (2015) 2064–2072.
[39] Y. Huang, M. Zhong, Y. Huang, M. Zhu, Z. Pei, Z. Wang, Q. Xue, X. Xie, C. Zhi, A self-healable and highly stretchable supercapacitor based on a dual crosslinked polyelectrolyte, Nat. Commun. 61 (2015) 10310.
[40] K. Takei, T. Takahashi, J.C. Ho, H. Ko, A.G. Gillies, P.W. Leu, R.S. Fearing, A. Javey, Nanowire active-matrix circuitry for low-voltage macroscale artificial skin, Nat. Mater. 910 (2010) 821–826.
[41] Y. Wu, L. Wang, X. Zhao, S. Hou, B. Guo, P.X. Ma, Self-healing supramolecular bioelastomers with shape memory property as a multifunctional platform for biomedical applications via modular assembly, Biomaterials 104 (2016) 18–31.
[42] Z. Yang, F. Wang, C. Zhang, J. Li, R. Zhang, Q. Wu, T. Chen, P. Sun, Bio-inspired self-healing polyurethanes with multiple stimulus responsiveness, Polym. Chem. 1024 (2019) 3362–3370.
[43] Y. Yanagisawa, Y. Nan, K. Okuro, T. Aida, Mechanically robust, readily repairable polymers via tailored noncovalent cross-linking, Science 3596371 (2018) 72–76.
[44] R. Du, Z. Xu, C. Zhu, Y. Jiang, H. Yan, H.-C. Wu, O. Vardoulis, Y. Cai, X. Zhu, Z. Bao, Q. Zhang, X. Jia, A highly stretchable and self-healing supramolecular elastomer based on sliding crosslinks and hydrogen bonds, Adv. Funct. Mater. 307 (2020), 1907139.
[45] K. Yu, H. Du, A. Xin, K.H. Lee, Z. Feng, S.F. Masri, Y. Chen, G. Huang, Q. Wang, Healable, memorizable, and transformable lattice structures made of stiff polymers, NPG Asia Mater. 121 (2020) 26.
[46] X. Qiu, Q. Cui, Q. Guo, T. Zhou, X. Zhang, M. Tian, Strong, healable, stimulus-responsive fluorescent elastomers based on assembled borate dynamic nanostructures, Small 1813 (2022), 2107164.

[47] A. Shabbir, I. Javakhishvili, S. Cerveny, S. Hvilsted, A.L. Skov, O. Hassager, N. J. Alvarez, Linear viscoelastic and dielectric relaxation response of unentangled upy-based supramolecular networks, Macromolecules 4910 (2016) 3899–3910.
[48] S. Perrier, 50th Anniversary Perspective: RAFT Polymerization—A User Guide, Macromolecules 5019 (2017) 7433–7447.
[49] T.F.A. de Greef, M.M.L. Nieuwenhuizen, R.P. Sijbesma, E.W. Meijer, Competitive intramolecular hydrogen bonding in oligo(ethylene oxide) substituted quadruple hydrogen bonded systems, J. Org. Chem. 753 (2010) 598–610.
[50] C.L. Lewis, M. Anthamatten, Synthesis, swelling behavior, and viscoelastic properties of functional poly(hydroxyethyl methacrylate) with ureidopyrimidinone side-groups, Soft Matter 915 (2013) 4058–4066.
[51] C. Heinzmann, I. Lamparth, K. Rist, N. Moszner, G.L. Fiore, C. Weder, Supramolecular polymer networks made by solvent-free copolymerization of a liquid 2-Ureido-4[1h]-pyrimidinone methacrylamide, Macromolecules 4822 (2015) 8128–8136.
[52] I. Schnell, B. Langer, S.H.M. Söntjens, R.P. Sijbesma, M.H.P. van Genderen, H. Wolfgang Spiess, Quadruple hydrogen bonds of ureido-pyrimidinone moieties investigated in the solid state by 1H double-quantum MAS NMR spectroscopy, Phys. Chem. Chem. Phys. 415 (2002) 3750–3758.
[53] K. Wendler, J. Thar, S. Zahn, B. Kirchner, Estimating the hydrogen bond energy, J. Phys. Chem. A 11435 (2010) 9529–9536.
[54] D. Wan, Q. Jiang, Y. Song, J. Pan, T. Qi, G.L. Li, Biomimetic tough self-healing polymers enhanced by crystallization nanostructures, ACS Appl. Polym. Mater. 22 (2020) 879–886.
[55] A. Ghosh, S. Samanta, S. Ge, A.P. Sokolov, K.S. Schweizer, Influence of attractive functional groups on the segmental dynamics and glass transition in associating polymers, Macromolecules 556 (2022) 2345–2357.
[56] M. Golkaram, G. Portale, P. Mulder, D. Maniar, S. Faraji, K. Loos, Order–disorder transition in supramolecular polymer combs/brushes with polymeric side chains, Polym. Chem. 1115 (2020) 2749–2760.
[57] M. Yamaguchi, Rheological properties of linear and crosslinked polymer blends: relation between crosslink density and enhancement of elongational viscosity, J. Polym. Sci. B Polym. Phys. 392 (2001) 228–235.
[58] S.H.M. Söntjens, R.P. Sijbesma, M.H.P. van Genderen, E.W. Meijer, Stability and lifetime of quadruply hydrogen bonded 2-Ureido-4[1H]-pyrimidinone dimers, J. Am. Chem. Soc. 12231 (2000) 7487–7493.
[59] M.J. Webber, M.W. Tibbitt, Dynamic and reconfigurable materials from reversible network interactions, Nat. Rev. Mater 77 (2022) 541–556.
[60] F. Meng, R.H. Pritchard, E.M. Terentjev, Stress relaxation, dynamics, and plasticity of transient polymer networks, Macromolecules 497 (2016) 2843–2852.
[61] J. Cui, A.d. Campo, Multivalent H-bonds for self-healing hydrogels, ChemComm 4874 (2012) 9302–9304.
[62] Y. Yang, M.W. Urban, Self-healing of polymers via supramolecular chemistry, Adv. Mater. Interfaces 517 (2018), 1800384.
[63] C.C. Hornat, M.W. Urban, Shape memory effects in self-healing polymers, Prog. Polym. Sci. 102 (2020), 101208.
[64] Y. Yang, M.W. Urban, Self-healing of glucose-modified polyurethane networks facilitated by damage-induced primary amines, Polym. Chem. 81 (2017) 303–309.
[65] Q. Zhang, S. Niu, L. Wang, J. Lopez, S. Chen, Y. Cai, R. Du, Y. Liu, J.-C. Lai, L. Liu, C.-H. Li, X. Yan, C. Liu, J.B.H. Tok, X. Jia, Z. Bao, An elastic autonomous self-healing capacitive sensor based on a dynamic dual crosslinked chemical system, Adv. Mater. 3033 (2018), 1801435.
[66] V. Iberi, I. Vlassiouk, X.G. Zhang, B. Matola, A. Linn, D.C. Joy, A.J. Rondinone, Maskless lithography and *in situ* visualization of conductivity of graphene using helium ion microscopy, Sci. Rep. 51 (2015) 11952.
[67] E. Mitterreiter, Y. Liang, M. Golibrzuch, D. McLaughlin, C. Csoklich, J.D. Bartl, A. Holleitner, U. Wurstbauer, A.S. Bandarenka, In-situ visualization of hydrogen evolution sites on helium ion treated molybdenum dichalcogenides under reaction conditions, npj 2D Mater. Appl. 31 (2019) 25.
[68] H. Ying, Y. Zhang, J. Cheng, Dynamic urea bond for the design of reversible and self-healing polymers, Nat. Commun. 51 (2014) 3218.
[69] G.M.L. van Gemert, J.W. Peeters, S.H.M. Söntjens, H.M. Janssen, A.W. Bosman, Self-healing supramolecular polymers in action, Macromol. Chem. Phys. 2132 (2012) 234–242.
[70] F.H. Beijer, R.P. Sijbesma, H. Kooijman, A.L. Spek, E.W. Meijer, Strong dimerization of ureidopyrimidones via quadruple hydrogen bonding, J. Am. Chem. Soc. 12027 (1998) 6761–6769.
[71] T.F.A. de Greef, G. Ercolani, G.B.W.L. Ligthart, E.W. Meijer, R.P. Sijbesma, Influence of selectivity on the supramolecular polymerization of ab-type polymers capable of both a·a and a·b interactions, J. Am. Chem. Soc. 13041 (2008) 13755–13764.
[72] X. Lin, Q. Xie, C. Ma, G. Zhang, Self-healing, highly elastic and amphiphilic silicone-based polyurethane for antifouling coatings, J. Mater. Chem. B 95 (2021) 1384–1394.
[73] C. Shao, M. Wang, L. Meng, H. Chang, B. Wang, F. Xu, J. Yang, P. Wan, Mussel-inspired cellulose nanocomposite tough hydrogels with synergistic self-healing, adhesive, and strain-sensitive properties, Chem. Mater. 309 (2018) 3110–3121.
[74] J. Herzberger, J.M. Sirrine, C.B. Williams, T.E. Long, Polymer Design for 3D Printing Elastomers: recent Advances in Structure, Properties, and Printing, Prog. Polym. Sci. 97 (2019), 101144.
[75] Q. Shi, K. Yu, X. Kuang, X. Mu, C.K. Dunn, M.L. Dunn, T. Wang, H. Jerry Qi, Recyclable 3D printing of vitrimer epoxy, Mater. Horiz. 44 (2017) 598–607.
[76] W. Niu, Z. Zhang, Q. Chen, P.-F. Cao, R.C. Advincula, Highly recyclable, mechanically isotropic and healable 3d-printed elastomers via polyurea vitrimers, ACS Mater. Lett. 38 (2021) 1095–1103.
[77] B. Zhang, K. Kowsari, A. Serjouei, M.L. Dunn, Q. Ge, Reprocessable thermosets for sustainable three-dimensional printing, Nat. Commun. 91 (2018) 1831.
[78] S. Kim, A. Rahman Md, M. Arifuzzaman, B. Gilmer Dustin, B. Li, K.Wilt Jackson, E. Lara-Curzio, T. Saito, Closed-loop additive manufacturing of upcycled commodity plastic through dynamic cross-linking, Sci. Adv. 822 (2022) eabn6006.
[79] E.B. Stukalin, L.-H. Cai, N.A. Kumar, L. Leibler, M. Rubinstein, Self-healing of unentangled polymer networks with reversible bonds, Macromolecules 4618 (2013) 7525–7541.
[80] F. Kremer, Andreas Schönhals, Broadband Dielectric Spectroscopy, Springer Science & Business Media, 2002.
[81] S. Samanta, S. Kim, T. Saito, A.P. Sokolov, Polymers with dynamic bonds: adaptive functional materials for a sustainable future, J. Phys. Chem. B 12533 (2021) 9389–9401.